Received: 20 October 2021 | Revised: 21 December 2021 | Accepted: 30 December 2021

DOI: 10.1002/aoc.6586

FULL PAPER

Applied Organometallic Chemistry WILEY

Sol–gel method synthesized Ce-doped TiO_2 visible light photocatalyst for degradation of organic pollutants

Mangesh G. Bhosale[1,2] | **Radhakrishna S. Sutar**[1] | **Swati S. Londhe**[3] | **Meghshyam K. Patil**[1]

[1]Department of Chemistry, Dr. Babasaheb Ambedkar Marathwada University, Aurangabad, Sub-Campus, Osmanabad, India

[2]Department of Chemistry, Ramkrishna Paramhansa Mahavidyalaya, Osmanabad, India

[3]K. T. Patil College of Pharmacy, Osmanabad, India

Correspondence
Meghshyam K. Patil, Department of Chemistry, Dr. Babasaheb Ambedkar Marathwada University, Aurangabad, Sub-Campus, Osmanabad, India.
Email: mkpatil.chemistryobad@bamu.ac.in; meghshyam_patil@yahoo.com

The Ce-doped TiO_2 nanoparticles were prepared by the sol–gel method. The prepared nanoparticles were characterized by sophisticated analytical techniques such as XRD, FESEM with EDX, HR-TEM, XPS, FTIR, TGA, and UV–visible spectroscopy, which gives structural features, morphology, elemental composition, and thermal stability of prepared nanoparticles. Based on the analysis, we conclude that increasing the dopant content of cerium in TiO_2 results in a decrease in particle size, increase in thermal stability, and decrease in band gap. Further, on increasing the dopant content of cerium, there is an increase in photocatalytic activity due to changes in structural features due to doping, and 5 mol% Ce-doped TiO_2 has shown nearly four times higher photocatalytic activity than pure TiO_2 for degradation of tetracycline. In this study, the photocatalytic activity and kinetics of photocatalytic degradation of antibacterial agent tetracycline have been studied by using these prepared catalysts. Further, effects of different parameters such as change in pH and change in concentration of tetracycline and amount of catalyst loading have been studied for the degradation of tetracycline. Also, Ce-doped TiO_2 has shown good photocatalytic efficiency for degradation of a mixture of textile dyes (methylene blue, rhodamine B, and brilliant green) and for degradation of a mixture of emerging contaminants (tetracycline, diclofenac, and triclosan).

KEYWORDS
Ce-doped TiO_2, nanoparticles, photocatalytic activity, sol–gel method, tetracycline

1 | INTRODUCTION

In last few decades, industrial evolution facilitated the humankind in different fields, but it also resulted in water as well as air pollution. Accretion of waste by-products from industries is mostly responsible for the water pollution, as mostly focus of the industries on the commercial product produced and harmful by-products are ignored. These by-products are mostly leaves to the water sources.[1,2] The main sources of water pollution includes industrially used dyes, pharmaceutical products, pesticides, fertilizers, and emerging contaminants, which are responsible for several health problems to humans and also disturbing the aquatic life. Several research groups all over the globe are working to treat the effluent from industries and on the degradation of organic pollutants in water. Several different techniques have been used for the treatment of different organic pollutants in

water.[3–6] One of the useful green technique for waste treatment is solar light-driven photocatalytic degradation of organic pollutants. Titanium dioxide (TiO_2), especially nano-sized TiO_2, has been severely explored for photocatalytic degradation of different organic pollutants. TiO_2 is associated with several characteristics/properties such as stability of its chemical structure, high surface area, biologically and chemically inertness, biocompatibility, physical properties, nontoxicity, low cost, and high oxidizing power.[7–12]

In 1964, the first photocatalytic oxidation of tetralin (1,2,3,4-tetrahydronaphthalene) by using TiO_2 suspension has been reported by Kato et al.[13] Thereafter in 1965, TiO_2 has been examined for the photocatalytic oxidation of ethylene and propylene.[14] Nevertheless, the most significant innovation that widely promoted the field of photocatalysis was the "Honda–Fujishima effect" mainly described in 1972 by Fujishima and Honda.[15] This invention starts the new era of photocatalysis. Thereafter, by taking motivation from these inventions, worldwide several research groups have utilized TiO_2 for photocatalytic reactions; some notable examples in early days are reduction of CN^- in water[16]; reduction of molecular nitrogen to ammonia and hydrazine over iron-doped TiO_2[17]; desert sand, and minerals to reduce nitrogen[18,19]; and so on.

Though TiO_2 has been explored much for the photocatalysis, it has some loopholes, which are responsible for the less efficiency of TiO_2 as a catalyst. These loopholes include (i) less reusability of catalyst; (ii) at more concentrations accumulation tendency of nano-sized TiO_2 suspension, leading to greater recombination rate of photoelectrons (e^-) and holes (h^+); (iii) less photocatalytic degradation efficacy of bare nano-sized TiO_2 in wastewater; and (iv) higher band gap (3.2 eV).[20–22]

One of the simple techniques to overcome these shortcomings is doping of TiO_2 with some element (metal or nonmetal). The metal doping can introduce a new hybrid energy level in the surface or bulk phase of TiO_2, thereby reducing its band gap energy and improving the separation efficiency of photo-generated electron–hole pairs.[23] Different metals such as V, Cr, Fe, Co, Mn, Mo, Ni, Cu, and Ce can be used for TiO_2 doping.[24–32] Further, for this purpose, different nonmetals can also be used as dopant, such as nitrogen, carbon, phosphorus, boron, and iodine.[33–37] For our study, we have selected ceria as a dopant. Several reports are available in the literature on the Ce-doped TiO_2, by using different preparative methods.[38–41] On the basis of the researcher's study, it has been observed that some of the methods involve tedious procedure, high-temperature treatment, and higher reaction time. The procedure applied in the present work is better or comparable to the literature. The cerium doping has expected much more attention due to the following reasons: (i) The redox couple Ce^{3+}/Ce^{4+} makes cerium oxide shift between CeO_2 and Ce_2O_3 under oxidizing and reducing conditions[42]; (ii) the easy formation of labile oxygen vacancies with the relatively high mobility of bulk oxygen species; and (iii) various photocatalytic properties caused by various ions (Ce^{3+}/Ce^{4+}). Also, Ce ions stay in the interstitial positions due to larger ionic radii of Ce^{3+} (1.15 Å) than Ti^{4+} (0.62 Å). Even Ce ions are larger than the diameter of the pure TiO_2, so they stay at the surface of nanocrystals rather than incorporated in the lattice.[43] Further, along with nano-size of the catalyst, the synergistic effect of cerium in the catalysts also played an important role in the enhancement of photocatalytic performance.

In the present work, different Ce-doped TiO_2 catalysts have been prepared by using simple sol–gel technique. These prepared catalysts have been characterized by using x-ray diffraction (XRD), infrared (IR), field emission scanning electron microscopy (FESEM) with energy-dispersive x-ray analysis (EDAX), transmission electron microscopy (TEM), and high-resolution transmission electron microscopy (HRTEM). Further, these catalysts have been successfully employed for the solar light-assisted photocatalytic degradation of organic dyes and some emerging contaminants.

2 | EXPERIMENTAL PROCEDURE

2.1 | Synthesis of Ce-doped TiO_2 nanoparticles

The Ce-doped TiO_2 nanoparticles were prepared by using sol–gel method. Firstly, 5 ml of titanium isopropoxide and 5 ml of glacial acetic acid were taken in a clean round-bottom flask; this mixture was stirred for 15 min. Separately, solution of surfactant Tween 80 in 10 ml distilled water has been prepared and slowly added to the solution of titanium isopropoxide and glacial acetic acid with constant stirring for 2 h. Further, to this 80 ml of distilled water was slowly added with constant stirring for 2 h. The stoichiometric amount of ceric ammonium nitrate as a dopant of Ce was added in a reaction mixture. The whole mixture was stirred for 4 h. To attend the pH 10 of the reaction mixture, 10% ammonia solution was added with constant stirring. After attending a pH, formed gel was digested for 3 h at 60°C, which also helps to remove excess ammonia. The reaction mixture was cooled to room temperature, precipitate has been settled down, and supernatant liquid has been removed and precipitate has been collected by filtration. Formed precipitate has been successively washed for three times with

distilled water and ethanol and dried at 110°C for 1 h. Finally, obtained product was ground to fine powder and calcined at 400°C for 5 h. Slightly yellowish powder of Ce-doped TiO_2 nanoparticles has been obtained.

By this procedure, we have prepared pure TiO_2, 1 mol %, 3 mol%, and 5 mol% Ce-doped TiO_2 nanoparticles.

2.2 | Characterization

The crystalline structure was characterized by XRD using Rigaku diffractometer with Cu Ka (1.5418 Å). The XRD data were recorded for 2θ range from 20° to 80° at scanning rate of 2°/min. FESEM with EDX analysis of the samples has been carried out to study the surface morphology and elemental composition by using the FESEM equipped with EDX using Carl Zeiss Supra 55. Further, HRTEM was performed using JEOL JEM 2100 Plus. Thermal stability of the prepared catalysts has been studied by thermogravimetric analysis (TGA). For band gap measurement, the UV–visible absorption spectra of prepared nanoparticles were recorded in the range of 200–800 nm by using Elico double beam UV–visible spectrophotometer (model no. SL 210). The XPS measurement of the prepared sample has been carried out on Shimadzu (ESCA 3400) spectrometer using Mg Kα (1253.6 eV) as a source of radiation excitation.

2.3 | Photocatalytic activity

Photocatalytic degradation of antimicrobial tetracycline in aqueous solution has been studied by employing prepared catalysts. Further, degradation of mixture of three dyes (includes brilliant green, rhodamine B, and methylene blue) and mixture of three emerging contaminants (includes tetracycline, diclofenac, and triclosan) in aqueous solution under direct sunlight has been studied by using most active 5 mol% Ce-doped TiO_2. Also, we have checked the effect of various parameters on photocatalytic efficiency of 5 mol% Ce-doped TiO_2 for degradation of tetracycline such as pH of the solution, concentration of the tetracycline, and catalyst loading. The pH of solution was adjusted by adding appropriate quantity of 0.1 N NaOH and 0.1 N HCl solutions.

2.3.1 | Photocatalytic degradation of antimicrobial tetracycline

We have prepared 200 ml of 20 ppm tetracycline solution using distilled water at room temperature. This prepared stock solution of tetracycline was taken in round-bottom flask; 100 mg of prepared catalyst has been added. This reaction mixture was stirred for 30 min in dark to reach adsorption desorption equilibrium. After this, the solution was transferred in to sunlight. Sample of 2 ml has been collected after regular time interval and performed UV–visible spectral analysis from 200 to 800 nm wavelengths, and absorbance has been recorded for wavelength 357 nm for tetracycline.

2.3.2 | Photocatalytic degradation of mixture of emerging contaminants

We have prepared 20 ppm solutions of tetracycline, triclosan, and diclofenac using distilled water. By taking these three solutions in equal quantity, 200 ml solution of mixture of tetracycline, triclosan, and diclofenac has been prepared. This solution was taken in round-bottom flask, and 100 mg 5 mol% Ce-doped TiO_2 catalyst was added to it. The reaction mixture was stirred for 30 min in dark to attain adsorption desorption equilibrium. After 30 min, the reaction mixture was transferred to direct sunlight; after regular time interval, the samples were collected. The absorbance of collected samples was recorded using UV–visible spectrophotometer at the range of 200–800 nm wavelengths.

2.3.3 | Photocatalytic degradation of mixture of dyes

We have prepared 20 ppm solutions of brilliant green, methylene blue, and rhodamine B using distilled water. By taking these three solutions in equal quantity, 200 ml solution of mixture of brilliant green, methylene blue, and rhodamine B has been prepared. This solution was taken in round-bottom flask, and 100 mg 5 mol% Ce-TiO_2 catalyst was added. After 30 min, the reaction mixture was transferred to direct sunlight; after regular time interval, the samples were collected. The absorbance of collected samples was recorded using UV–visible spectrophotometer at the range of 200–800 nm wavelengths.

3 | RESULT AND DISCUSSIONS

3.1 | TGA

Prior to calcination, the TGA of bare TiO_2 and Ce-doped TiO_2 has been studied, and obtained results are shown in Figure 1. Both the samples have shown the four weight losses. First weight loss has occurred from ambient temperature to 100°C, which is due to loss of physically

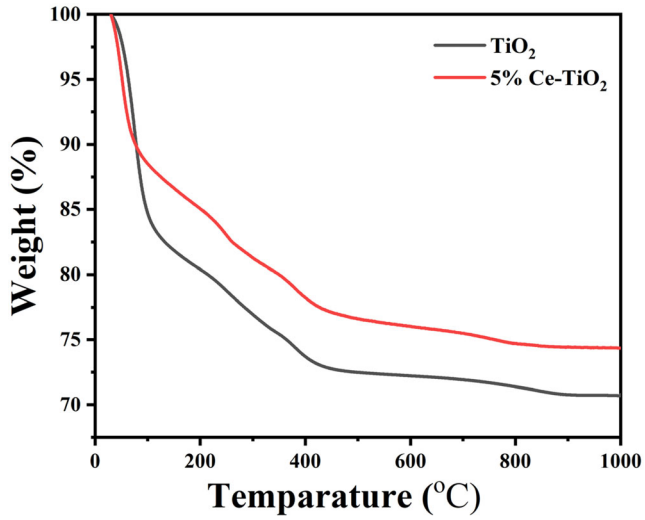

FIGURE 1 TGA of TiO_2 and Ce-TiO_2

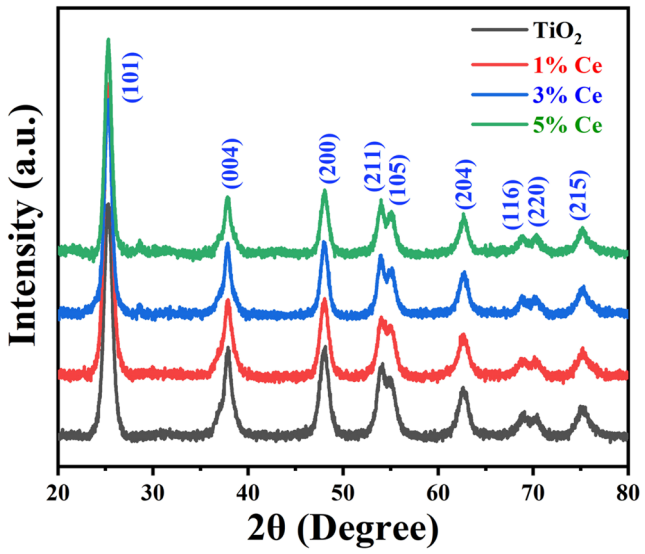

FIGURE 2 XRD pattern of pure TiO_2 and Ce-doped TiO_2 samples

adsorbed moisture, and corresponding weight loss for TiO_2 and Ce-doped TiO_2 was found to be 12% and 16%, respectively. Second weight loss has been observed from the temperature 100 to 200°C, which is relatively minor weight loss and found to be 3%–4% for both samples. This weight loss corresponds to the conversion of hydroxides into their corresponding amorphous oxides.[44] The third weight loss is due to loss of coordinated water as well as organic moieties, observed for the samples from 200 to 400°C. The fourth weight loss has been occurred for temperature range 400–800°C, which is relatively less (<5%) for both the sample, and it suggests that TiO_2 and Ce-doped TiO_2 catalysts are stable gravimetrically as well as thermally at higher temperature. However, at further higher temperature (up to 1000°C), there is no weight loss. The overall weight loss from ambient temperature to 1000°C has been found to be 29% and 25% for bare TiO_2 and 5% Ce-doped TiO_2, respectively. The decrease in weight loss on incorporating cerium into TiO_2 suggests that doping of cerium results in increase in thermal stability of the catalyst.

3.2 | XRD analysis

The XRD study of all prepared samples shows the formation of anatase phase of TiO_2 and crystalline in nature (Figure 2). Further, no other phase of TiO_2 such as rutile or brookite has been formed.[45] The diffraction peaks present at (2θ values) 25.28°, 37.92°, 48.14°, 54.21°, 54.88°, 62.56°, 69.03°, 70.43°, and 74.98° correspond to planes (101), (004), (200), (211), (105), (204), (116), (220), and (215), respectively. All these angles and corresponding planes have resemblance with the JCPDS No. 73-1764, which shows the presence of pure anatase phase. Further, it suggests that tetragonal structure of TiO_2 has been retained after doping as well.[36,46] The ionic radii of Ce^{3+} (0.111 nm) and Ce^{4+} (0.101 nm) are greater than Ti^{4+} (0.068 nm); it is difficult for Ce^{3+} and Ce^{4+} to convert Ti^{4+} into a crystal lattice. Further, no crystalline phase related to cerium oxides has been found, confirming the inclusion of all Ce in the TiO_2 structure. On the other hand, a new peak appears for the 3 mol% and 5 mol% doped samples at 28.61°. If it came from the newly formed peak of TiO_2, it should appear in all the samples. But it did not comply to the results obtained, so it should be related to cerium oxide instead of TiO_2. According to the diffraction angle of that new peak, it can be sequenced in the CeO_2 phase, indicating that an important portion of the Ce^{3+} ion was oxidized in Ce^{4+} during the heat treatment.[47]

The crystalline size of all samples has been calculated by Scherrer equation 1 using the most intense peak at (101) plane. The crystalline size of bare TiO_2, 1% Ce–TiO_2, 3% Ce–TiO_2, and 5% Ce–TiO_2 is found to be 9.92, 8.57, 8.24, and 8.15 nm, respectively. Doping of Ce in TiO_2 results in decrease in crystalline size of the catalyst.

$$D = k\lambda/\beta\cos\theta \quad (1)$$

where D is average size of nanoparticle, λ is the wavelength, β is the full width at half maximum, and θ is Bragg's angle. The structural parameters are shown in Table 1, which are well matching with JCPDS data of pure TiO_2.

TABLE 1 Structural parameters of pure TiO_2 and Ce-doped nanoparticles

Catalysts	Standard d value	Observed d value	hkl plane	Cell parameters			Crystallite size (nm)
				a(Å)	c(Å)	V(Å^3)	
TiO_2	3.52	3.5147	(101)	3.78	9.52	136.02	9.927933
	2.37	2.38018	(004)				
	1.33	1.89052	(220)				
1% Ce–TiO_2	3.52	3.5147	(101)	3.78	9.50	135.73	8.57579
	2.37	2.37533	(004)				
	1.33	1.89497	(220)				
3% Ce–TiO_2	3.52	3.51607	(101)	3.77	9.48	135.25	8.245584
	2.37	2.37171	(004)				
	1.33	1.88868	(220)				
5% Ce–TiO_2	3.52	3.5188	(101)	3.78	9.49	135.59	8.158314
	2.37	2.37352	(004)				
	1.33	1.89089	(220)				

3.3 | FTIR studies

Figure 3 shows that FTIR spectroscopic study of Ce-doped TiO_2 nanoparticles. All the samples have shown a broad absorption band at 3369 cm^{-1}, which corresponds to the O–H stretching vibration of adsorbed moisture on the surface of the catalyst.[48] The absorption band at 2348 cm^{-1} corresponds to the vibrational bond energy of CO_2, whereas the weak absorption band at 1633 cm^{-1} belongs to the vibrational bond energy of C=O. The small absorption bands at about 1428 and 1357 cm^{-1} might be originated from the C–O stretching vibration, and bands at about 1160 cm^{-1} is probably due to the C–O–C alkoxy stretching due to presence of small residues of organic part from the precursors. The absorption band at 973 cm^{-1} shows the vibration of Ce–O, and the band at 547 cm^{-1} is due to TiO_2.[46] The spectra of Ce-doped TiO_2 samples are slightly different from that of TiO_2. Nearly all absorption bands are slightly shifted to lower wave number, which may happened due to small atomic weight of Ce. All of these changes in the spectra of Ce-doped TiO_2 indicate that Ce has taken place of Ti in TiO_2 lattice.

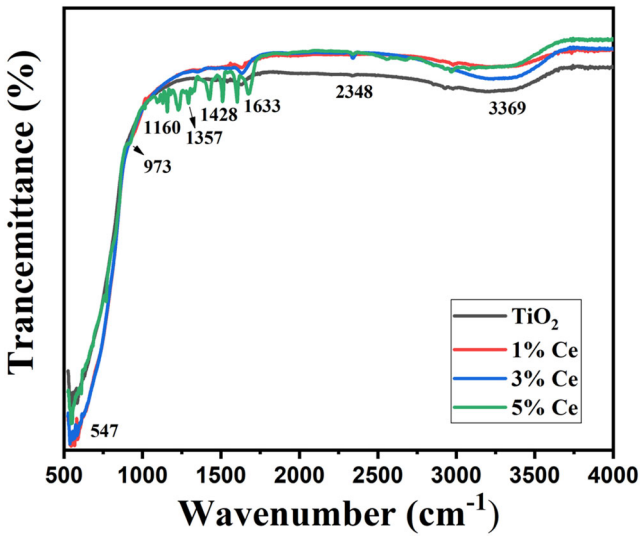

FIGURE 3 FTIR study of Ce–TiO_2 nanoparticles

3.4 | FESEM and HRTEM studies

The morphology and surface nature of the synthesized Ce-doped TiO_2 nanoparticles were studied by FESEM, and obtained images of all samples are shown in Figure 4. The FESEM micrograph of all samples has shown the well-grown crystals, which were accumulated closely with each other. Further, the EDX analysis has shown that samples have similar elemental composition as per proportion of precursors taken during the preparation (Table 2). Further, we have supplied more FESEM images of all prepared catalysts in Figure S1.

HRTEM analysis has been shown that the average particle size of the prepared catalysts is in the range of 8–11 nm (Figure 5a), and it well matches with XRD calculations. At higher magnification, the inter-planar spacing is found to be 0.351 nm, which corresponds to the (101) plane of anatase TiO_2[49] (Figure 5b). The selected area electron diffraction (SAED) pattern of Ce–

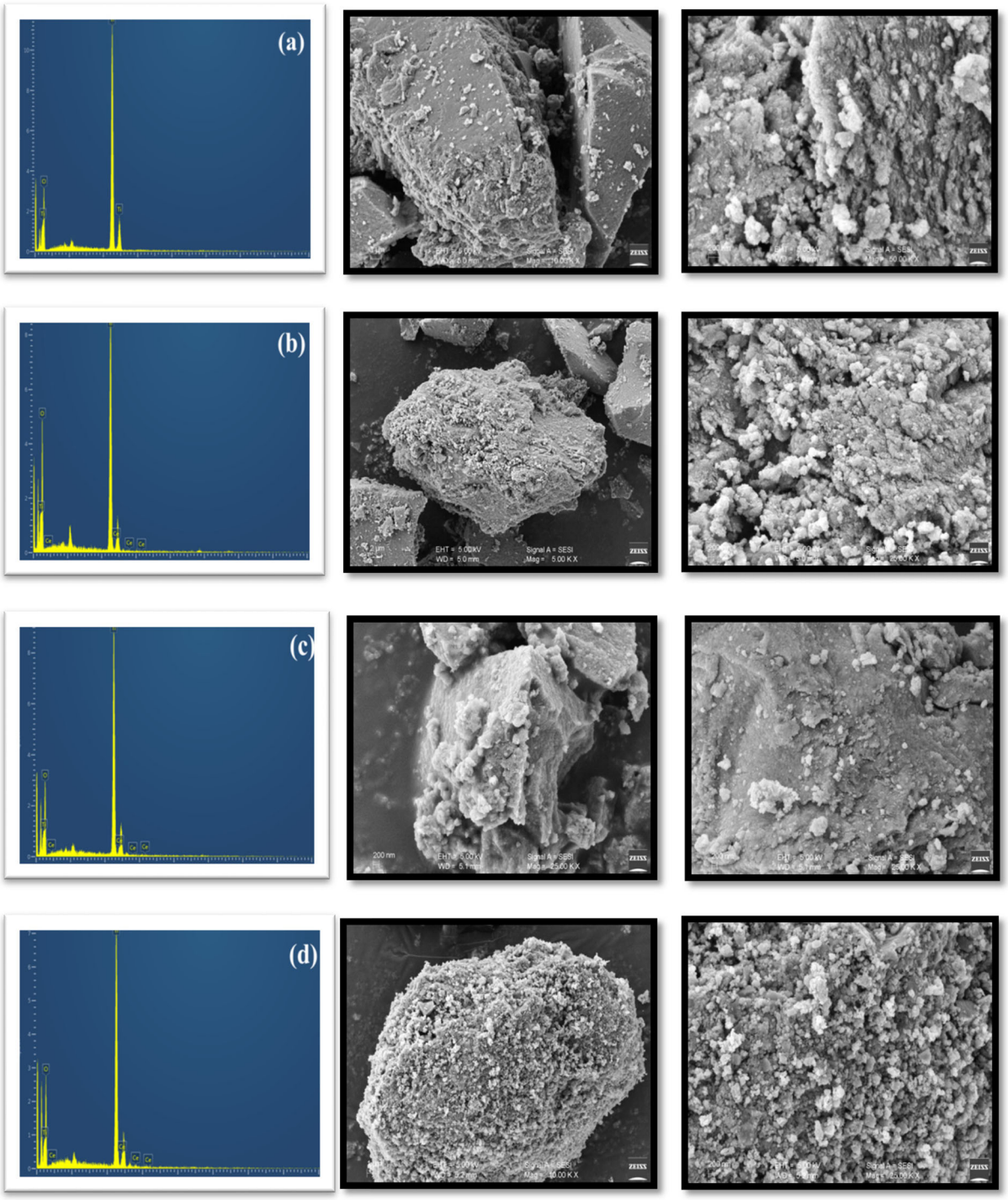

FIGURE 4 FESEM with EDX of (a) pure TiO_2, (b) 1 mol% Ce-doped TiO_2, (c) 3 mol% Ce-doped TiO_2, and (d) 5 mol% Ce-doped TiO_2

TiO_2 nanoparticles has been shown in Figure 5c, which further confirms the anatase phase of TiO_2 and well matches with XRD data. The lightening and intensity of polymorphic rings in SAED pattern confirm the crystalline nature of nanoparticles.[50] Figure 5d shows the uniform distribution of nano-sized particles. Further, we have supplied more HRTEM images of 5 mol% Ce-doped in Figure S2.

3.5 | UV–visible absorption study

UV–visible absorption spectra of the prepared samples have been shown in Figure 6a. Ce-doped samples have shown the stronger absorption edge and shifted to the upper wavelength than pure TiO_2. This confirms that doping of Ce in TiO_2 shifted the absorption edge to higher wavelength and reduces the band gap. The spectra

shift more to the visible region with the increasing amount of Ce in Ce–TiO_2 materials. Furthermore, a great rise within the absorption was observed between 3.6 and 3.0 eV, which increases with increasing Ce loading (Figure 6b). Figure 6 shows the dependence of the absorption edge on the Ce loading. It indicates that the photocatalytic activity observed in the visible region of electromagnetic spectrum.[46] Ce-doped TiO_2 can enhance the absorption in visible region because of the certain 4f electronic configuration of cerium, which is a creator of electron–hole pairs to improve the visible light response.[51]

TABLE 2 Weight percent of elements in the prepared samples

		Weight % of elements		
Sr. no.	Sample	Oxygen	Titanium	Cerium
1	TiO_2	49.86	50.14	-
2	1% Ce–TiO_2	43.16	56.06667	0.78
3	3% Ce–TiO_2	48.67	48.8775	2.445
4	5% Ce–TiO_2	51.96	44.34	3.7

3.6 | X-ray photoelectron spectroscopy

The XPS analysis of 5% Ce-doped TiO_2 is demonstrated in Figure 7, which confirms the elemental composition of as-prepared catalyst. Figure 7a shows the survey spectra, which indicates the presence of Ti, Ce, and O in the sample. The Ce 3d high-resolution scan spectrum is shown in Figure 7b. The peaks located at 904.2 and 885.5 eV corresponds to Ce $3d_{3/2}$ and Ce $3d_{5/2}$, respectively, indicating that Ce exists to include TiO_2 in the grid, mainly in the form of Ce^{3+}. The doping concentration of Ce is very low, and the characterized peaks of Ce element are weak. As shown in Figure 7c, peaks at 458.61 and 464.42 eV correspond to Ti $2p_{3/2}$ and Ti $2p_{1/2}$, respectively, which are higher than pure TiO_2 (Ti $2p_{3/2}$ 458.5 eV and Ti $2p_{1/2}$ 464.2 eV). This may be due to the lower electronegativity of Ce than Ti, which gives higher electron binding energy.[52] Figure 7d shows the O 1s high-resolution XPS scan spectrum. The strong peak at 529.8 eV top arises from the overlapping contributions of oxygen from TiO_2 and Ce–O–Ti compounds in which oxygen is the primary contributor to TiO_2.[53]

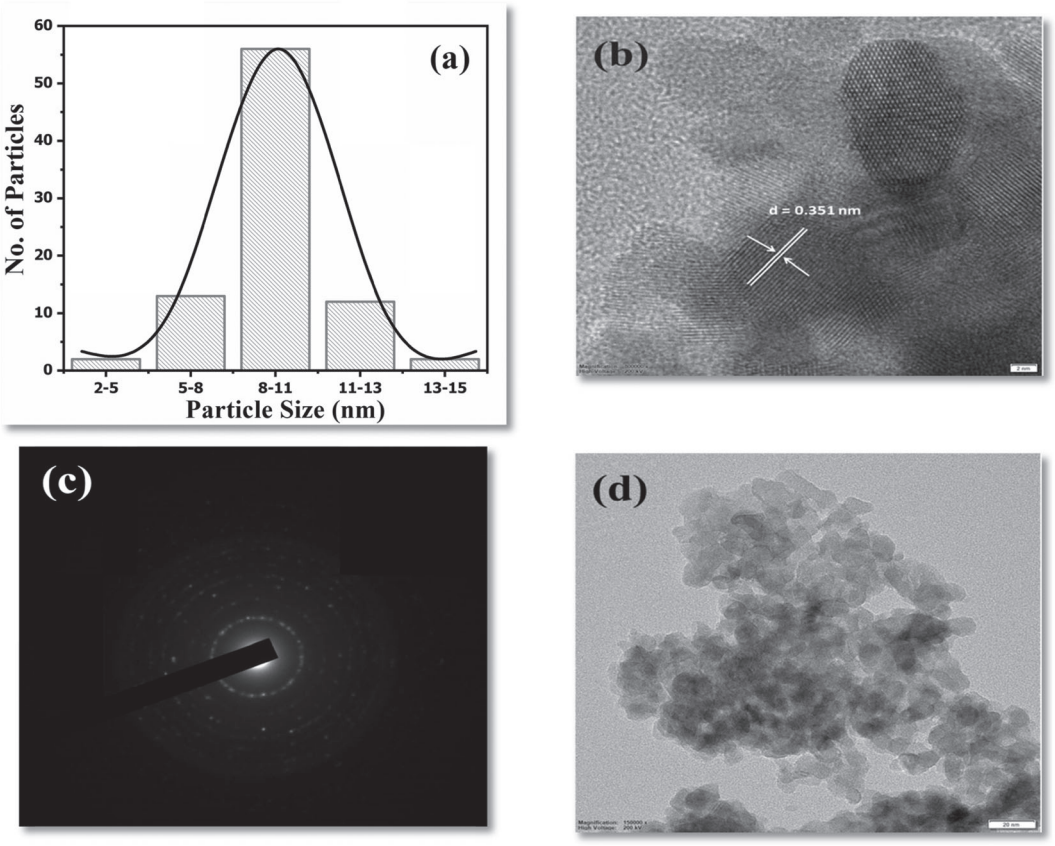

FIGURE 5 (a) Average particle size, (b) HRTEM image, (c) SAED pattern, (d) HRTEM image (at different magnification) of 5% Ce–TiO_2 powder

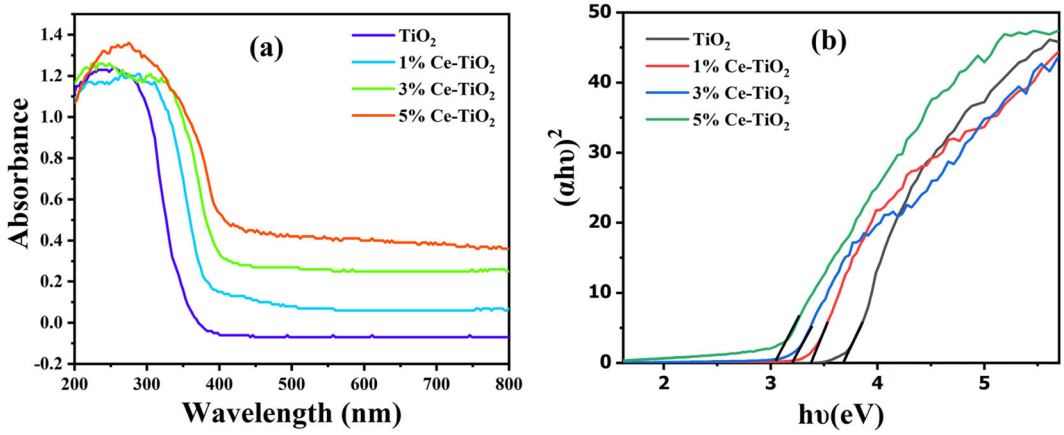

FIGURE 6 (a) UV–Visible absorption spectra. (b) Plot of hυ Vs $(\alpha h\upsilon)^2$ of bare TiO_2 and Ce-doped TiO_2

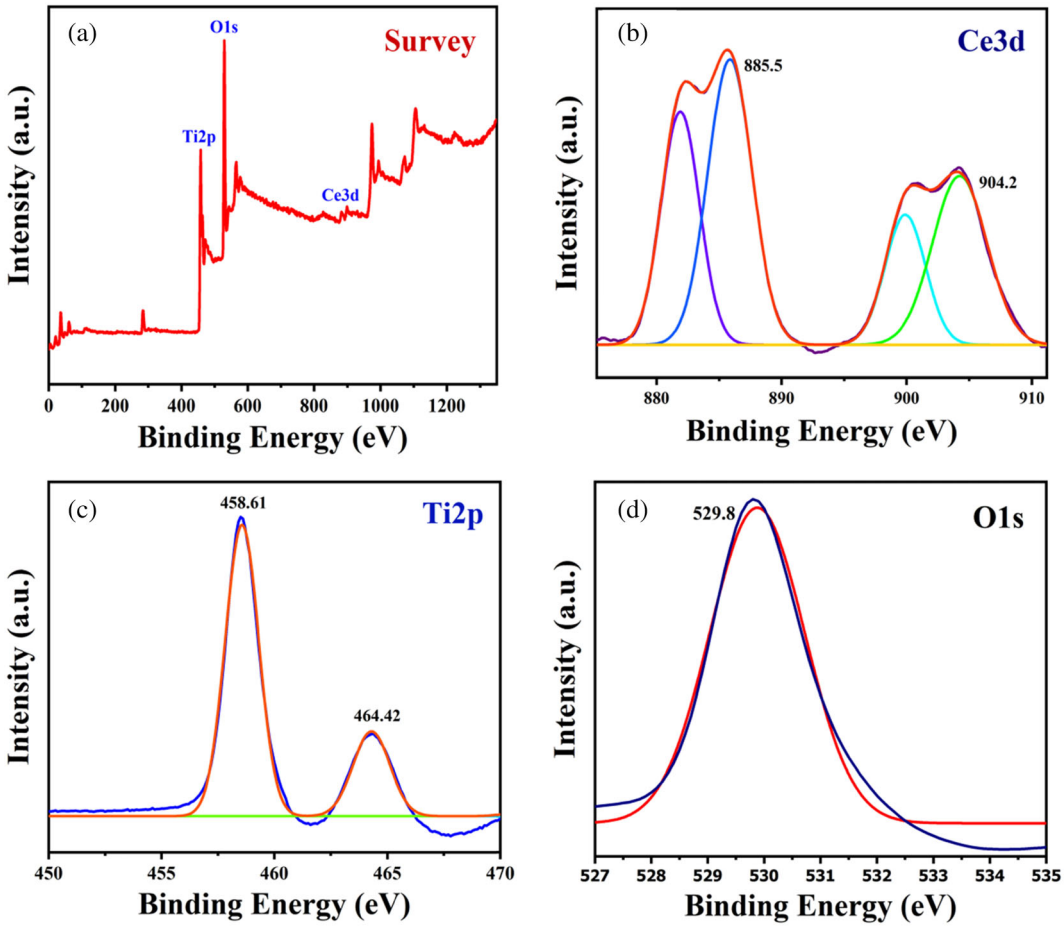

FIGURE 7 (a) XPS spectra of 5% Ce-doped TiO_2, high-resolution spectra of (b) Ce 3d, (c) Ti 2p, (d) O 1s

4 | PHOTOCATALYTIC ACTIVITY

The photocatalytic activity of prepared catalysts was carried for degradation of organic pollutant tetracycline under direct sunlight. Further, the best working catalyst i.e. 5 mol% Ce-doped TiO_2 in the prepared series has been explored for the degradation of mixture of dyes (viz., BG, RB, and MB) and mixture of emerging contaminants (viz., TC, DCF, and triclosan). In addition, the effect of different parameters such as pH and concentration of tetracycline and catalyst loading was studied briefly for photodegradation of tetracycline

by using 5 mol% Ce-doped TiO_2 catalyst under direct sunlight.

4.1 | Photocatalytic degradation of tetracycline

The representative UV–visible spectra of samples collected during photocatalytic degradation of tetracycline using 5 mol% Ce-doped TiO_2 catalyst is shown in Figure 8a. The intensity of characteristic absorption peaks at wavelengths (λ_{max}) 274 and 356 nm of tetracycline has been decreased gradually with irradiation time. Figure 8b,c shows the comparative study of photocatalytic degradation of tetracycline using bare TiO_2 and Ce-doped TiO_2 catalysts. The complete degradation of tetracycline was observed in 120 min by using 1 mol% Ce-doped TiO_2, and it takes 60 min for 5 mol% Ce-doped TiO_2. It shows that 5% Ce–TiO_2 catalyst is the most prominent catalyst for degradation.

Kinetic plot for photodegradation reaction of tetracycline for the different catalysts with respect to varying irradiation time is shown in Figure 8c. The concentration of tetracycline was nearly constant in the absence of photocatalyst (only under direct sunlight), indicating the negligible photodegradation of TC without catalyst. In the absence of sunlight, catalyst can adsorb TC, which is only about 5% in initial 30 min, and keeping in dark for longer time, no further adsorption is observed. It suggests that tetracycline is very much stable in the absence of catalyst or light. With irradiation time of 60 min, nearly complete degradation of TC (~93%) was observed by using 5% Ce-TiO_2, whereas 78.68%, 64.8%, and 42.67% degradation was observed by using 3% Ce–TiO_2, 1% Ce–TiO_2, and TiO_2, respectively. 5% Ce–TiO_2 has shown higher photocatalytic activity in less time as compared with other catalysts. This observation clearly indicates that photocatalytic reaction is highly dependent on the amount of Ce doped in TiO_2. The higher activity of 5 mol % Ce-doped TiO_2 is due to its lower crystalline size and

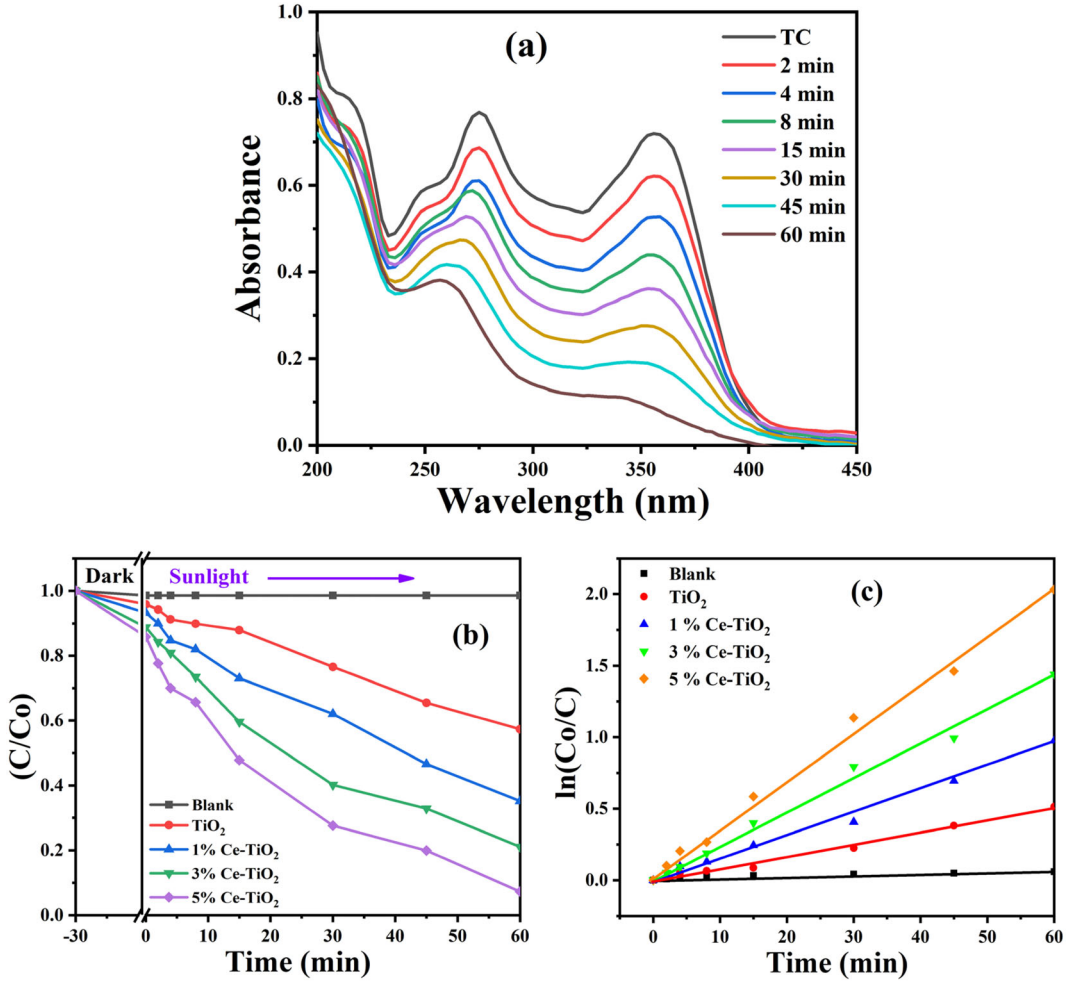

FIGURE 8 Photodegradation of TC by catalysts: (a) UV–visible spectra of TC, (b) kinetic plot of C/C_0 versus time, (c) corresponding graph of $\ln(C_0/C)$ versus time

lower band gap as compared with other prepared catalysts. As discussed earlier, 5 mol% Ce-doped TiO_2 has crystalline size of about 8.15 nm, whereas other prepared catalysts such as 3 mol% Ce-doped TiO_2, 1 mol% Ce-doped TiO_2, and TiO_2 have crystalline size of 8.24, 8.57, and 9.92 nm, respectively. Furthermore, 5% Ce-TiO_2 has lowest band gap ($E_{bg} = 2.80$ eV) than other prepared catalysts.

In the photodegradation studies, the apparent rate constant was applied because it consents for the independent determination of photocatalytic activity of the previous adsorption period. The apparent first-order kinetic equation is given as follows:

$$-log\frac{C_o}{C} = K_{app}\frac{t}{2.303} \quad (2)$$

where K_{app} is the apparent rate constant of a reaction, C_o is the initial concentration of dye solution at $t = 0$, and C is the remaining concentration of dye solution at time t.[50]

Table 3 shows the reaction kinetic parameters for degradation of TC using different catalysts. The 5 mol% Ce-doped TiO_2 has the highest rate constant (88.65×10^{-3} min^{-1}) compared with other catalysts. Rate constant for 5 mol% Ce-doped TiO_2 is more than four time than prepared TiO_2. Figure 8c shows that plot of ln (C_o/C) versus time, which is straight line passing through origin. It shows that this photocatalytic degradation follows first-order kinetic reaction.

Due to better activity of 5 mol% Ce-doped TiO_2, we have selected this catalyst to study the different parameters of photodegradation, that is, effect pH of the solution, concentration of TC, and amount of catalyst loading. To study the effect of TC concentration on the photocatalytic degradation, the experiments were studied by taking 10, 20, 30, and 40 ppm of TC solution. In this study, 200 ml of TC solution was taken in round-bottom flask, and 100 mg 5 mol% Ce-doped TiO_2 catalyst was added. From the graph of (C/C_o) against given time interval (shown in Figure 9a), degradation of 10 ppm solution has been completed within 30 min, whereas other solutions required much more time for complete degradation, and only 72%, 56%, and 32% degradation has been achieved in 30 min for 20, 30, and 40 ppm solution, respectively.

Further, plot ln (C_o/C) against time is straight line (Figure 9b) passing through origin showing that photodegradation reaction follows the first-order kinetics. The plot of change in concentration of dye per unit time, that is, (d[TC]/dt) versus irradiation time, is shown in Figure 9c. In general, rate of degradation per unit time increases with increase in the concentration of organic pollutant, as more number of molecules are available for degradation; on the other hand, increase in the concentration of organic pollutant restricts the incoming light to reach and consequently decreases the rate of degradation per unit time. The net result of these two effects is responsible for the rate of degradation. On increasing the concentration from 10 to 20 ppm up to irradiation time 4 min, the rate of degradation increases, whereas on further increasing the concentration up to 40 ppm, the rate slightly decreases. For irradiation time 4–30 min, the rate of degradation increases from 10 to 30 ppm and slightly decreased for 40 ppm as compared with 30 ppm solution.

The photodegradation efficiency of the catalyst depends on the pH of the solution. Therefore, we have studied degradation of TC at various pH of the solution, namely, 3, 5, 9, and 12. In this study, we have observed that solutions having basic pH require less time for complete degradation than solutions with acidic pH (Figure 10a). Change in pH (acidic or basic) changes the surface charge on catalyst and the strength of photocatalytic reactions. The reactive species $OH^{\bullet}$, $O_2^{\bullet -}$, and $HO_2^{\bullet}$ are responsible for the photocatalytic degradation. These active radicals are responsible for degradation as shown in Equations 3–8. At basic pH, activity is superior as compared with acidic pH, suggesting that the $OH^{\bullet}$ radical plays an important role during the degradation. Further, plot of ln(C_0/C) versus time of irradiation for all pH is straight line passing through the origin, which shows that reaction follows the first-order reaction kinetics at all pH (Figure 9b). Equation 3–8 show the general mechanism of photodegradation of TC.

The photocatalytic degradation efficiency was evaluated by changing catalyst loading of 5% Ce-doped TiO_2 from 0.25 g/L to 1 g/L for TC solution and illustrated in Figure 11a,b. The result shows that the rate of catalytic

TABLE 3 Reaction kinetic parameters for degradation of TC by using prepared catalysts

Catalyst	Initial conc. of TC (%)	Final conc. of TC (%)	Rate constant min^{-1}
Blank	100	98.8	00.40×10^{-3}
TiO_2	100	57.33	18.54×10^{-3}
1% Ce–TiO_2	100	35.2	34.81×10^{-3}
3% Ce–TiO_2	100	21.32	51.52×10^{-3}
5% Ce–TiO_2	100	7	88.65×10^{-3}

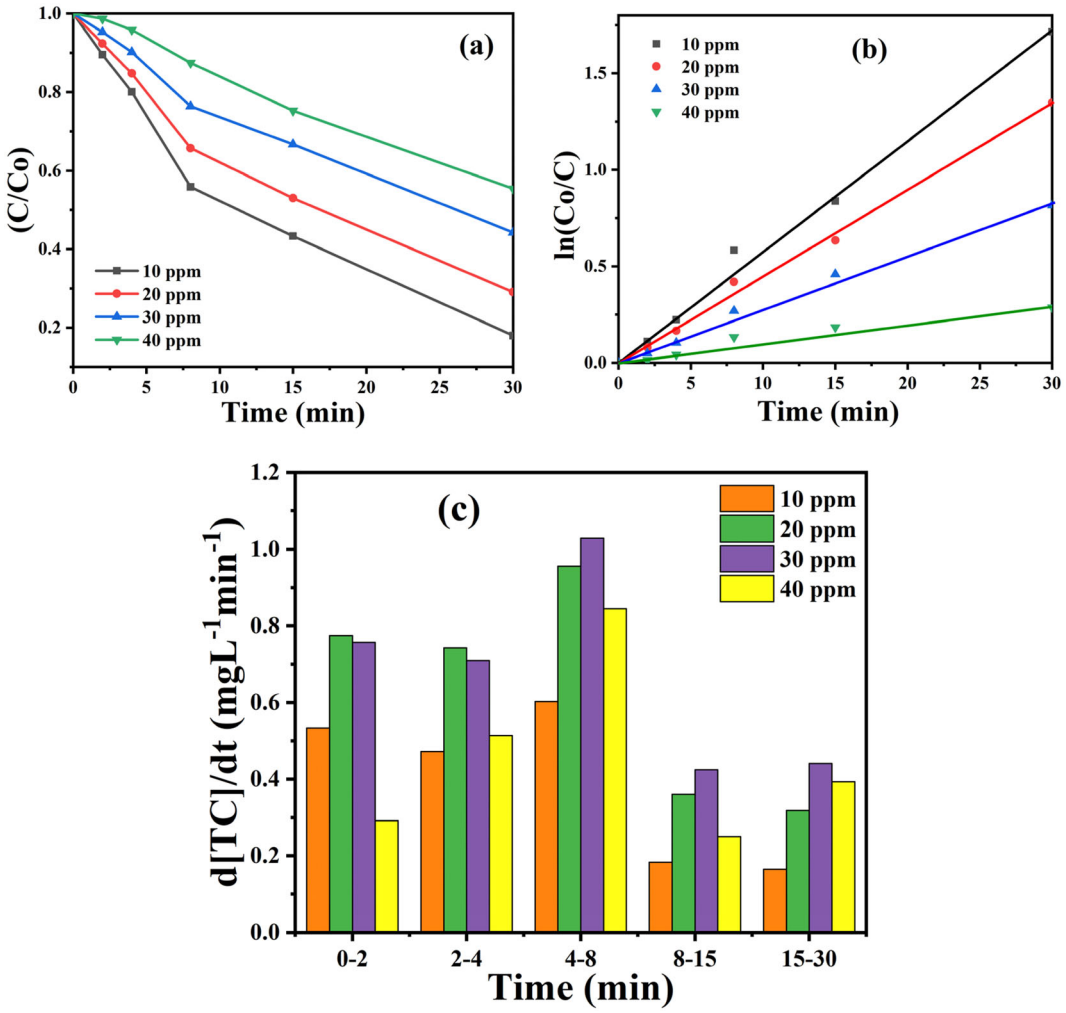

FIGURE 9 Photocatalytic degradation of TC for different concentrations of dye: (a) plot of C/C_0 versus time, (b) plot of $\ln(C_0/C)$ versus time, (c) plot of d[TC]/dt versus time

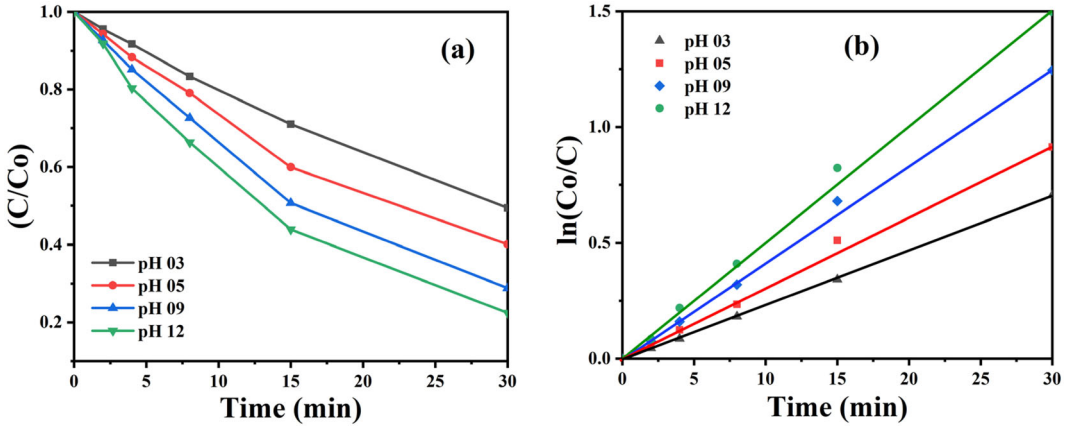

FIGURE 10 pH variations on photocatalytic degradation: (a) C/C_0 against change in time, (b) ln (C_0/C) against change in time

reaction increases with increase in amount of catalyst loading, as the presence of higher amount of catalyst offers greater active surface area and sites, which are involved in the degradation reaction. Also, due to increase in catalyst loading, adsorption of dye on the surface of catalyst also increases.

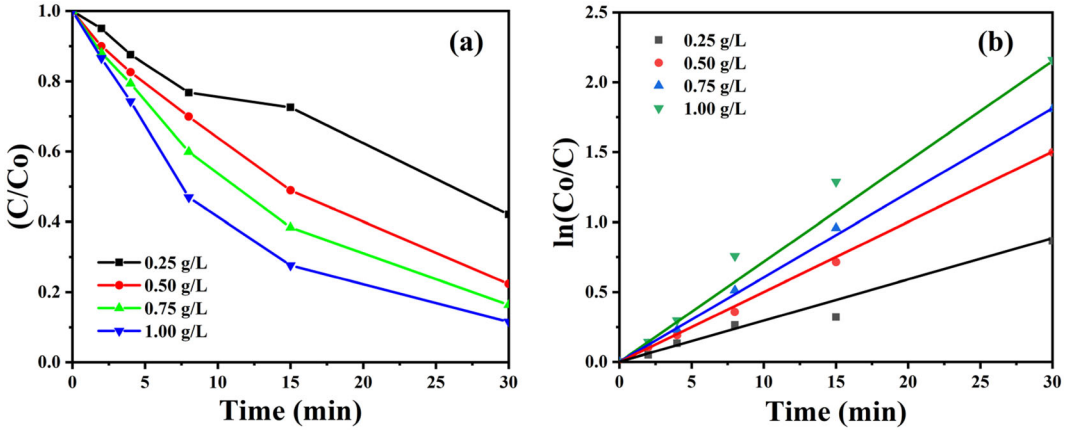

FIGURE 11 Photocatalytic degradation of TC with different weights of catalyst: (a) (C/C_0) against irradiation time, (b) ln (C_0/C) against irradiation time

$$Ce-TiO_2+hv\rightarrow Ce-TiO_2\left(e^-+h^+\right) \quad (3)$$

$$Ce-TiO_2\left(h^+\right)+H_2O\rightarrow\ HO^\bullet+h^++Ce-TiO_2 \quad (4)$$

$$Ce-TiO_2\left(h^+\right)+OH^-\rightarrow HO^\bullet+Ce-TiO_2 \quad (5)$$

$$Ce-TiO_2(e^-)+O_2\rightarrow O_2^{\bullet-}+Ce-TiO_2 \quad (6)$$

$$Ce-TiO_2(e^-)+O_2+h^+\rightarrow HO_2^\bullet+Ce-TiO_2 \quad (7)$$

$$TC+Active\ radicals\left(\mathrm{OH}^\bullet,\mathrm{O}_2^{\bullet-},\mathrm{HO}_2^\bullet\right)\rightarrow Degradation\ products \quad (8)$$

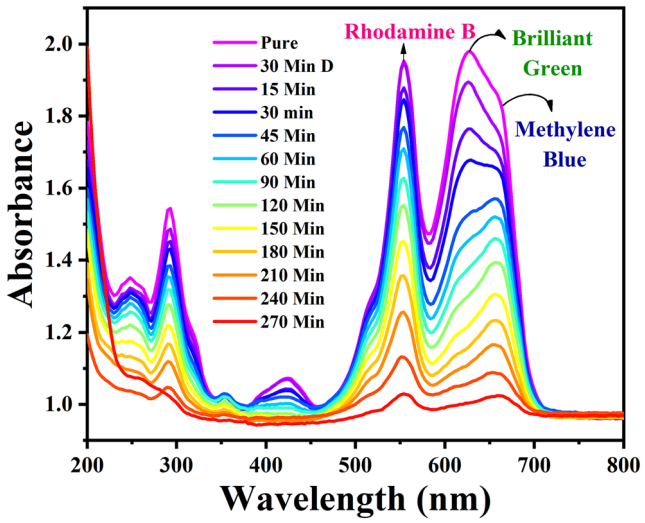

FIGURE 12 Plot of absorbance against wavelength of photocatalytic degradation of mixture of dyes (MB, BG, and RB)

4.2 | Degradation of mixture of dyes

Most of textile industries produce lot of waste having mixture of dyes. Therefore, a lot of study have been carried out on the degradation of dye using photocatalysts.[24–37,54–57] In this study, we have taken mixture of dyes as a representative of industrial effluent. To study the degradation of mixture of dyes, we have taken a 200 ml, 20 ppm solution of mixture of dyes, namely, brilliant green, methylene blue, and rhodamine B, and 100 mg of best working catalyst 5 mol% Ce-doped TiO_2. This reaction mixture was kept in dark for 30 min to attain adsorption desorption equilibrium. Further, the solution is kept in sunlight, and samples were analysed in the given time interval on UV–visible spectrophotometer. Corresponding absorbance against wavelength plot for degradation of mixture of dyes using 5 mol% Ce-doped TiO_2 is shown in Figure 12. The plots for 3 mol% Ce-doped TiO_2, 1 mol% Ce-doped TiO_2, and pure TiO_2 have been shown in Figure S3. These plots have shown absorption peaks at wavelengths (λ_{max}) 665, 625, and 560 nm, which correspond to characteristics λ_{max} of methylene blue, brilliant green, and rhodamine B, respectively. As irradiation time increases, absorbance decreases, and almost complete degradation of these three dyes has taken place in 270 min by using 5 mol% Ce-doped TiO_2 catalyst.

4.3 | Mixture of emerging contaminants

To study the degradation of mixture of emerging contaminants, we have taken a 200 ml, 20 ppm solution mixture of emerging contaminants, namely, tetracycline,

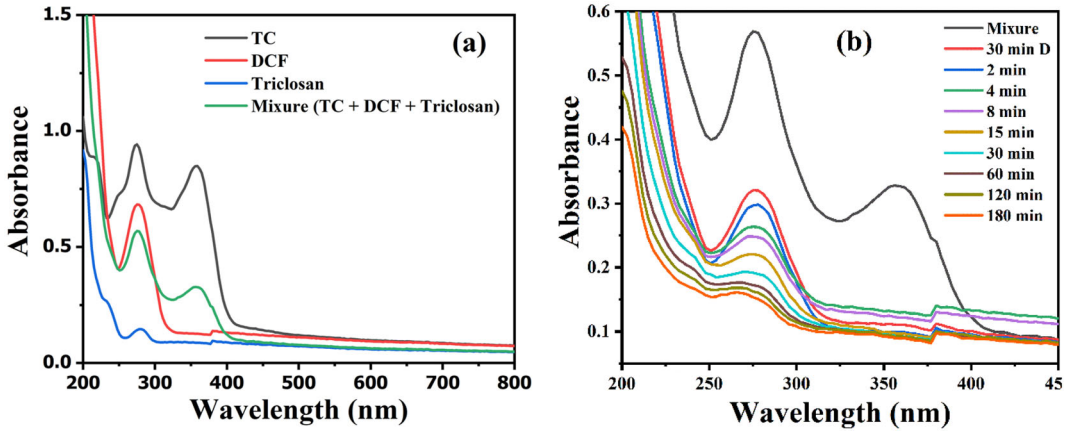

FIGURE 13 Photocatalytic degradation of mixture (triclosan, TC, and DCF)

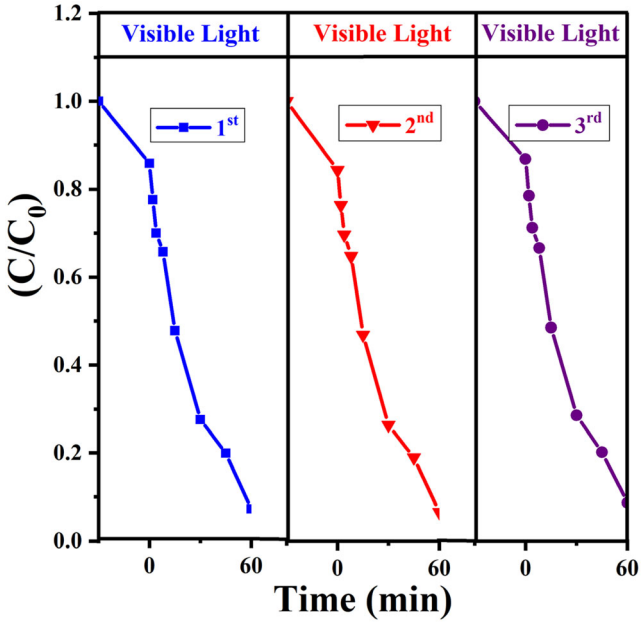

FIGURE 14 Reusability of catalyst

triclosan, and diclofenac, and 100 mg of best working catalyst 5 mol% Ce-doped TiO_2. Figure 13a shows the UV–visible spectra of TC, DCF, and triclosan and their mixture in equal quantity. This plot shows the characteristic peaks of TC ($\lambda_{max} = 274$, 356 nm), DCF ($\lambda_{max} = 276$ nm), and triclosan ($\lambda_{max} = \sim 280$ nm). Further, as all three (TC, DCF, and triclosan) have one common λ_{max} at ~275 nm, in their mixture, this peak has approximately average of intensity from individual contaminant at this λ_{max}. This reaction mixture was kept in dark for 30 min to attain adsorption desorption equilibrium. Further, the solution is kept in sunlight, and samples were analyzed in the given time interval on UV–visible spectrophotometer from 200 to 450 nm. Correspondingly, absorbance versus wavelength plot is shown in Figure 13b. As irradiation time increases, absorbance decreases, and almost complete degradation of these three emerging contaminants has been taken place in 180 min.

5 | REUSABILITY OF CATALYST

The reusability of the prepared nanoparticles is the most important aspect for catalyst efficiency for practical reuse. Therefore, we performed photocatalytic degradation of tetracycline using 5 mol% Ce-doped TiO_2 for three cycles; the obtained results have been shown in Figure 14. The result of these experiments shows that the catalyst has outstanding reusability.

6 | CONCLUSIONS

Visible light active Ce-doped TiO_2 was successfully synthesized by using sol–gel method. Among the various nanoparticles, 5 mol% Ce–doped TiO_2 has shown better efficiency for photodegradation of tetracycline (TC). Further, it has been successfully employed for the degradation of mixture of three dyes, namely, methylene blue (MB), rhodamine B (RB), and brilliant green (BG), and mixture of emerging contaminants, namely, tetracycline (TC), triclosan, and diclofenac (DC). From the characterization of the catalysts, it has been confirmed that 5 mol% Ce–doped TiO_2 acts as a sensitizer in the photocatalytic degradation. However, strong interaction of Ce in TiO_2 has been proved by FTIR. From UV–visible absorption study, 5 mol% Ce–doped TiO_2 catalyst has shown better visible light absorption than other prepared catalysts. The band gaps 3.0, 3.1, 3.3, and 3.6 eV have been observed for 5 mol% Ce-doped TiO_2, 3 mol% Ce-doped TiO_2, 1 mol% Ce-doped TiO_2, and pure TiO_2, respectively. Also, 5 mol%

Ce-doped TiO_2 catalyst has shown almost similar efficiency for three cycles. Rate constant of 5 mol% Ce-doped TiO_2 catalyst is nearly twice to that of bare TiO_2 for degradation of tetracycline.

CONFLICT OF INTEREST

The authors declare that they have no conflict of interest.

AUTHOR CONTRIBUTIONS

Mangesh Bhosale: Investigation; project administration. **Radhakrishna Sutar:** Project administration. **Swati Londhe:** Project administration. **Meghshyam Patil:** Supervision.

DATA AVAILABILITY STATEMENT

Data available in article.

ORCID

Mangesh G. Bhosale https://orcid.org/0000-0002-1036-9018
Radhakrishna S. Sutar https://orcid.org/0000-0002-6131-3946
Swati S. Londhe https://orcid.org/0000-0002-1776-0079
Meghshyam K. Patil https://orcid.org/0000-0002-3144-5016

REFERENCES

[1] N. Ferronato, V. Torretta, *Int. J. Environ. Res. Public Health* **2019**, *16*, 1060.
[2] J. Gutberlet, A. M. Baeder, *Int. J. Environ. Health Res.* **2008**, *18*, 1.
[3] A. Maleki, M. Mohammad, Z. Emdadi, N. Asim, M. Azizi, J. Safaei, *Arab. J. Chem.* **2020**, *13*, 3017.
[4] J. Wang, Z. Wang, C. L. Z. Vieira, J. M. Wolfson, G. Pingtian, S. Huang, *Ultrason. Sonochem.* **2019**, *55*, 273.
[5] E. S. M. Mouele, J. O. Tijani, O. O. Fatoba, L. F. Petrik, *Environ. Sci. Pollut. Res.* **2015**, *22*, 18345.
[6] A. Maleki, *Ultrason. Sonochem.* **2018**, *40*, 460.
[7] L. Gomathi Devi, G. Krishnamurthy, *J. Hazard. Mater.* **2009**, *162*, 899.
[8] H. Yahiro, T. Miyamoto, N. Watanabe, H. Yamaura, *Catal. Today* **2007**, *120*, 158.
[9] M. N. Abellán, R. Dillert, J. Giménez, D. Bahnemann, *J. Photochem. Photobiol.* **2009**, *202*, 164.
[10] N. Venkatachalam, M. Palanichamy, B. Arabindoo, V. Murugesan, *J. Mol. Catal. A: Chem.* **2007**, *266*, 158.
[11] L.-C. Chen, C.-M. Huang, F.-R. Tsai, *J. Mol. Catal. A: Chem.* **2007**, *265*, 133.
[12] C. Xie, Z. Xu, Q. Yang, B. Xue, Y. Du, J. Zhang, *Mater. Sci. Eng.B.* **2004**, *112*, 34.
[13] S.-i. Kato, F. Masuo, *Kogyo Kagaku Zasshi* **1964**, *67*, 1136.
[14] I. S. McLintock, M. Ritchie, *J. Chem. Soc., Faraday Trans.* **1965**, *61*, 1007.
[15] A. Fujishima, K. Honda, *Nature* **1972**, *238*, 37.
[16] S. N. Frank, A. J. Bard, *J. Am. Chem. Soc.* **1977**, *99*, 303.
[17] G. Schrauzer, T. Guth, *J. Am. Chem. Soc.* **2002**, *99*, 7189.
[18] S. M. Gupta, M. Tripathi, *Chi. Sci. Bull.* **2011**, *56*, 1639.
[19] G. N. Schrauzer, N. Strampach, L. N. Hui, M. R. Palmer, J. Salehi, *Proc. Natl. Acad. Sci. U. S. a.* **1983**, *80*, 3873.
[20] N. F. Zainudin, A. Z. Abdullah, A. R. Mohamed, *J. Hazard. Mater.* **2010**, *174*, 299.
[21] A. Y. Shan, T. I. M. Ghazi, S. A. Rashid, *Appl Catal A-Gen.* **2010**, *389*, 1.
[22] M.-H. Baek, W.-C. Jung, J.-W. Yoon, J.-S. Hong, Y.-S. Lee, J.-K. Suh, *J. Ind. Eng. Chem.* **2013**, *19*, 469.
[23] C. Liu, X. Tang, C. Mo, Z. Qiang, *J. Solid State Chem.* **2008**, *181*, 913.
[24] S.-q. Wang, J.-m. Li, W.-b. Liu, *J. Fuel Chem. Technol.* **2020**, *48*, 1131.
[25] M. Shaban, A. M. Ahmed, N. Shehata, M. A. Betiha, A. M. Rabie, *J. Colloid Interface Sci.* **2019**, *555*, 31.
[26] A. Mancuso, O. Sacco, D. Sannino, S. Pragliola, V. Vaiano, *Arab. J. Chem.* **2020**, *13*, 8347.
[27] M. Mokhtari Nesfchi, A. Ebrahimian Pirbazari, F. E. Khalil Saraei, F. Rojaee, F. Mahdavi, S. A. Fa'al Rastegar, *Mater. Sci. Semicond. Process.* **2021**, *122*, 105465.
[28] A. Tab, M. Dahmane, C. Belabed, B. Bellal, C. Richard, M. Trari, *Sci. Total Environ.* **2021**, *780*, 146451.
[29] X. Zhang, W.-F. Chen, G. Bahmanrokh, V. Kumar, N. Ho, P. Koshy, C. C. Sorrell, *Nano-Struct. Nano-Objects* **2020**, *24*, 100557.
[30] A. Kaiba, O. Ouerghi, M. H. Geesi, A. Elsanousi, A. Belkacem, O. Dehbi, A. I. Alharthi, M. A. Alotaibi, Y. Riadi, *J. Mol. Struct.* **2020**, *1203*, 127376.
[31] S. Ahadi, N. S. Moalej, S. Sheibani, *Solid State Sci.* **2019**, *96*, 105975.
[32] I. Tbessi, M. Benito, E. Molins, J. Liorca, A. Touati, S. Sayadi, W. Najjar, *Solid State Sci.* **2019**, *88*, 20.
[33] Y. Wu, M. Xing, B. Tian, J. Zhang, F. Chen, *Chem. Eng. Sci.* **2010**, *162*, 710.
[34] Z. Noorimotlagh, I. Kazeminezhad, N. Jaafarzadeh, M. Ahmadi, Z. Ramezani, S. Silva Martinez, *J. Hazard. Mater.* **2018**, *350*, 108.
[35] Z. Zhang, C. Zhao, Y. Duan, C. Wang, Z. Zhao, H. Wang, Y. Gao, *Appl. Surf. Sci.* **2020**, *527*, 146693.
[36] R. P. Barkul, M. K. Patil, S. M. Patil, V. B. Shevale, S. D. Delekar, *J. Photochem. Photobiol.* **2017**, *349*, 138.
[37] L. Zhou, J. Deng, Y. Zhao, W. Liu, L. An, F. Chen, *Mater. Chem. Phys.* **2009**, *117*, 522.
[38] R. P. Barkul, F.-N. A. Shaikh, S. D. Delekar, M. K. Patil, *Curr. Nanosci.* **2017**, *13*, 110.
[39] A. M. T. Silva, C. G. Silva, G. Dražić, J. L. Faria, *Catal. Today* **2009**, *144*, 13.
[40] J. Y. Lee, J. H. Choi, *Materials (Basel).* **2019**, *12*, 1265.
[41] A. Jafari, S. Khademi, M. Farahmandjou, *Mater. Res. Express* **2018**, *5*, 095008.
[42] F. B. Li, X. Z. Li, M. F. Hou, K. W. Cheah, W. C. H. Choy, *Appl. Catal. A-Gen.* **2005**, *285*, 181.
[43] S. N. R. Inturi, T. Boningari, M. Suidan, P. G. Smirniotis, *Appl. Catal. B. Environ.* **2014**, *144*, 333.
[44] R. P. Barkul, V. B. Koli, V. B. Shewale, M. K. Patil, S. D. Delekar, *Mater. Chem. Phys.* **2016**, *173*, 42.
[45] N. Sofyan, A. Ridhova, A. H. Yuwono, A. Udhiarto, *Int. J. Technol.* **2017**, *8*, 1229.

[46] Z. N. Kayani, S. R. Maria, S. Naseem, *Ceram. Int.* **2020**, *46*, 381.
[47] J. Xie, D. Jiang, M. Chen, J. Di Li, X. Zhu, C. Y. Lü, *Colloids and Surfaces a: Physicochem. Eng. Aspects* **2010**, *372*, 107.
[48] A. Maleki, M. Rabbani, S. Shahrokh, *Appl. Organometal. Chem.* **2015**, *29*, 809.
[49] L. Gong, Z. Zhou, S. Wang, B. Wang, *Mater. Sci. Semicond. Process.* **2013**, *16*, 288.
[50] R. S. Sutar, R. P. Barkul, S. D. Delekar, M. K. Patil, *Arab. J. Chem.* **2020**, *13*, 4966.
[51] X. P. Cao, D. Li, W. H. Jing, W. H. Xing, Y. Q. Fan, *J. Mater. Chem.* **2012**, *22*, 15309.
[52] R. Xu, Y. Li, S. Feng, J. Wang, J. Zhang, X. Zhang, C. Bian, W. Fu, Z. Li, H. Yang, *J. Mater. Sci.* **2020**, *55*, 5681.
[53] N. Yan, Z. Zhu, J. Zhang, Z. Zhao, Q. Liu, *Mater. Res. Bull.* **2012**, *47*, 1869.
[54] M. H. Abdellah, S. A. Nosier, A. H. El-Shazly, A. A. Mubarak, *Alex. Eng. J.* **2018**, *57*, 3727.
[55] M. Jeyaraj, R. Atchudan, S. Pitchaimuthu, T. N. J. I. Edison, P. Sennu, *Process Saf. Environ. Prot.* **2021**, *156*, 457.
[56] R. Atchudan, T. N. J. I. Edison, S. Pitchaimuthu, R. Vinodh, Y. R. Lee, *J. Alloys Compd.* **2018**, *766*, 12.
[57] R. Atchudan, T. N. J. I. Edison, S. Perumal, D. Karthikeyan, Y. R. Lee, *J. Photochem. Photobiol., a* **2017**, *333*, 92.

SUPPORTING INFORMATION

Additional supporting information may be found in the online version of the article at the publisher's website.

How to cite this article: M. G. Bhosale, R. S. Sutar, S. S. Londhe, M. K. Patil, *Appl Organomet Chem* **2022**, e6586. https://doi.org/10.1002/aoc.6586